On a thermodynamically consistent flow model for induced anisotropy in polar ice

SWANTJE BARGMANN
TU Dortmund
Institute of Applied Mechanics
Dortmund, GERMANY
swantje.bargmann@tu-dortmund.de

HAKIME SEDDIK
Hokkaido University
Inst. Low Temp. Sci.
Sapporo, JAPAN
hakime@lowtem.hokudai.ac.jp

RALF GREVE
Hokkaido University
Inst. Low Temp. Sci.
Sapporo, JAPAN
greve@lowtem.hokudai.ac.jp

Abstract: A thermodynamically consistent flow model for induced anisotropy in polar ice has been introduced in [8, 11]. The so-called Continuum-mechanical, Anisotropic Flow model based on an anisotropic Flow Enhancement factor (CAFFE-model for short) is based on a generalization of the isotropic Glen's flow law. A scalar enhancement factor which takes the ice's anisotropy into account generalizes Glen's flow law for anisotropic materials. In this contribution, the CAFFE-model is applied to the EPICA ice core at Kohnen Station, Dronning Maud Land, Antarctica. Numerical results are presented and discussed.

Key–Words: polar ice, Antarctica, EDML, ice flow, anisotropy, continuum mechanics

1 Introduction

Antarctica is the Earth's southernmost continent and about 98 % of its surface are covered by thick ice masses. It is by far the largest single ice body on Earth and posseses a total ice volume of $29.5 \cdot 10^6$ km^3. Further, approximately $0.58 \cdot 10^6$ km^3 ice of ice shelves are attached to Antarctica.

Although usually natural ice is typically regarded as isotropic, this is not the case for thick ice masses [1, 4]. It consists of a vast number of small individual hexagonal crystallites ('ice I_h'). Whereas the distribution of the crystallographic axes is mainly random at the surface, deeper into the ice, the fabrics with preferred directions develop (cf. [6]). Moreover, one is dealing with two different length scales: the diameter of crystal which is usually of the unit millimeters to centimeters and the size of the ice masses which can be up to thousands of kilometers.

In the literature, there exist different models capable of describing the anisotropy of polar ice. On the one hand, some of those account for anisotropy via introducing an enhancement factor as a multiplier of the isotropic ice fluidity. These models are rather simple, however, the ad hoc introduction of the multiplier is physically questionable. On the other hand, there exist very complex full-field models which take many physical details into account. Yet, the increased complexity leads to a large increase in computational time. Therefore, the later approaches can usually not be included in a macroscopic ice flow model.

One model which is capable of modeling anisotropic ice flow and leads to a reasonable computational time is the macroscopic CAFFE model. Moreover, the CAFFE model fulfills all fundamental principles of classical continuum mechanics [7].
Here, the CAFFE model is applied to EPICA deep ice drilling site near Kohnen Station, Dronning Maud Land, Antarctica - referred to as the EDML core. EPICA, the European Project for Ice Coring in Antarctica, runs two deep ice core drilling sites in Antarctica. The EDML core was drilled between January 2002 and the beginning of 2006. A drilling depth of 2774.15 m was reached and the ice core stores information about the climatic changes during the last 150 000 years.
First, we reiterate the underlying ideas of the CAFFE model and its mathematical formulation. For a detailed introduction, the reader is referred to [8, 11]. Four different recrystallization effects are explained and incorporated in the model. Next, the anisotropic generalization of Glen's flow law is introduced in Section 2.2. Then, in order to demonstrate its performance, the CAFFE model is applied to the EDML deep drilling site in Antarctica. The underlying assumptions and conditions at EDML are stated and explained. Finally, numerical results are presented and compared to the data which is available for the EDML. In the end, we summarize the main findings.

2 The CAFFE model

The CAFFE model is a continuum mechanical theory which contains more information of the underlying microstructure that influences the macroscopic mate-

rial behavior. However, the microscopic level is not resolved and the information enters the macroscopic governing equations indirectly.

In order to take the microstructure into account a field quantity called orientation mass density ρ^* is introduced. In addition to the dependence on the position $\boldsymbol{x}$ and time $\boldsymbol{t}$, the orientation mass density ρ^* depends on the orientation $\boldsymbol{n}$ of the grain. The orientation $\boldsymbol{n}$ is the normal unit vector parallel to the crystal's c-axis in the unit sphere S^2. In the following, all quantities which additionally depend on the orientation $\boldsymbol{n}$ are denoted with "*".
The orientation mass density ρ^* is governed by the orientation mass balance

$$\frac{\partial \rho^*}{\partial t} + \operatorname{div}(\rho^* \boldsymbol{v}) + \operatorname{div}_{S^2}(\rho^* \boldsymbol{u}^*) = \rho^* \Gamma^*. \quad (1)$$

Here, $\boldsymbol{v}(\boldsymbol{x}, t)$ is the classical velocity and $\boldsymbol{u}^*(\boldsymbol{x}, t, \boldsymbol{n}) = \dot{\boldsymbol{n}}$ the orientation change velocity rate which describes the transition of mass with one orientation to another (neighboring) orientation on the unit sphere S^2. Furthermore, the orientation production rate is denoted by $\Gamma^*(\boldsymbol{x}, t, \boldsymbol{n})$.

2.1 Recrystallization effects

Via the orientation mass balance four different recrystallization effects are incorporated: (i) local rigid body rotation, (ii) grain rotation, (iii) rotation recrystallization and (iv) grain boundary migration. The later expresses that the fraction of grains with a certain orientation changes due to the fact that the boundary between two grains moves in favor of the better orientated grain and is modeled via the orientation production rate $\Gamma^*(\boldsymbol{x}, t, \boldsymbol{n})$

$$\Gamma^* = \Gamma_c \frac{A(T')}{A(-10°C)} \left[\mathcal{A}^* - \mathcal{A}\right], \quad (2)$$

following [8], and depends on the deformability $\mathcal{A}$ of the polycrystalline ice

$$\mathcal{A} = \int_{S^2} \mathcal{A}^*(\boldsymbol{n}) \frac{\rho^*(\boldsymbol{x}, t, \boldsymbol{n})}{\rho(\boldsymbol{x}, t)} \, \mathrm{d}^2 n \quad (3)$$

and the deformability

$$\mathcal{A}^* = \left[[\boldsymbol{S} \cdot \boldsymbol{n}]^2 - [\boldsymbol{n} \cdot \boldsymbol{S} \cdot \boldsymbol{n}]^2 \right] / \operatorname{tr}\left(\boldsymbol{S}^2\right) \quad (4)$$

of a single crystal. For a detailed physical explanation on the definition of the deformabilities, the reader is referred to [11]. $\boldsymbol{S}$ is the deviatoric part of the Cauchy stress. The remaining symbols in Eq. (2) represent the constant material parameter Γ_c and the rate factor $A(T')$ which is given by the Arrhenius law

$$A(T') = A_0 \exp(-\frac{Q}{RT'}). \quad (5)$$

Here, A_0 is the pre-exponential constant, Q denotes the activation energy and R is the universal gas constant. Moreover, the rate factor $A(T')$ depends on the temperature relative to pressure melting $T' = T + \beta p$, where T is the absolute temperature and $\beta = 9.8 \cdot 10^{-2}$ K/MPa being the Clausius–Clapeyron constant for ice [6]. In general, the melting point of ice is lowered by approximately 1 K per kilometer of ice thickness.

The local rigid body rotation (rbr), grain rotation (gr) and rotation recrystallization (rc) effects are mapped via the the orientation change velocity rate

$$\begin{aligned} \boldsymbol{u}^*(\boldsymbol{x}, t, \boldsymbol{n}) &= \boldsymbol{u}^*_{\mathrm{rbr}} + \boldsymbol{u}^*_{\mathrm{gr}} + \boldsymbol{u}^*_{\mathrm{rc}} \\ &= \boldsymbol{W} \cdot \boldsymbol{n} + \iota [[\boldsymbol{n} \cdot \boldsymbol{D} \cdot \boldsymbol{n}] \, \boldsymbol{n} - \boldsymbol{D} \cdot \boldsymbol{n}] + \frac{\boldsymbol{q}^*}{\rho^*}, \end{aligned} \quad (6)$$

with $\boldsymbol{W}$ and $\boldsymbol{D}$ being the strain rate and the spin tensor, respectively. The first term describes the contribution of the polycrystal's local rigid body rotation to the orientation transition rate. The second term $\boldsymbol{u}^*_{\mathrm{gr}}$ maps the physical effect of grain rotation with the help of the shape factor ι. Last but not least, the effect of rotation recrystallization is described by the orientation flux $\boldsymbol{q}^*$. It refers to the process that subgrain boundaries develop due to formations of dislocations in heterogeneous loading cases [5, 9]. Some grains are better orientated for dislocation slip than others. During the deformation process grains can break apart at these subgrain boundaries and the emerging new grains will have slightly different orientations. Consequently, it is a diffusive process and is described by Fick's law of diffusion

$$\boldsymbol{q}^* = -\lambda \nabla^* \rho^*, \quad (7)$$

with λ being the diffusivity.

2.2 Non-classical, anisotropic Glen's flow law

As usual, we approximate ice as an incompressible and extremely viscous non-Newtonian fluid. Originally, Glen's flow law has been formulated for the isotropic case. Due to the induced anisotropy in thick ice masses, it must be enhanced. The anisotropic generalization of Glen's flow law reads

$$\boldsymbol{D} = A(T') \hat{E}(\mathcal{A}) \left[\sqrt{\left[\operatorname{tr}(\boldsymbol{S}^2)\right] / 2} \right]^{n-1} \boldsymbol{S}, \quad (8)$$

following [8, 11]. Here, n is the same stress exponent as in the case of the classical flow law by Glen. Experiments, e.g. [2], show that the scalar anisotropic enhancement factor $\hat{E}(\mathcal{A})$ depends on the square of the deformability $\mathcal{A}$ in the interval $[1, 2.5]$. Furthermore,

we require that the enhancement factor $\hat{E}$ is a strictly monotonically increasing function of the deformability $\mathcal{A}$ and continuously differentiable and, therefore, propose:

$$\hat{E}(\mathcal{A})=\begin{cases} E_{\min}+[1-E_{\min}]\,\mathcal{A}^{\frac{8}{21}\frac{E_{\max}-1}{1-E_{\min}}}, \\ \qquad\qquad \text{if } 0\le\mathcal{A}\le 1, \\ \frac{4\mathcal{A}^2[E_{\max}-1]+25-4E_{\max}}{21}, \\ \qquad\qquad \text{if } 1\le\mathcal{A}\le 2.5 \end{cases} \tag{9}$$

The two parameters $E_{\min}$ and $E_{\max}$ are known from experiments. In this contribution, we use the values $E_{\max}=10$ and $E_{\min}=0$ for the maximum softening and hardening parameters, respectively.

3 Application to Antarctica's deep drilling site EDML

Following Seddik et al. [11], we apply a coordinate system whose origin lies in the center of the drilling site. The x-axis points in direction of the ice divine (260-west-southwest direction) and the y-axis in 170-south-southeast direction. Consequently, the z-axis points vertically downwards. Moreover, due to this choice, we obtain the following approximation for the gradient of the free surface elevation h

$$\frac{\partial h}{\partial x}=-9\cdot 10^{-4}\pm 10\%, \qquad \frac{\partial h}{\partial y}=0. \tag{10}$$

Thus, the only non-vanishing shear-stress component S_{xz} reads

$$S_{xz}=\rho g z\frac{\partial h}{\partial x}, \tag{11}$$

where g is the acceleration due to gravity and the mass density of ice reads $\rho=910\ \mathrm{kg\,m^{-3}}$. Combination with the x-z-component of the anisotropic Glen's flow law (8) and subsequent integration over the z-component yields the anisotropic horizontal velocity

$$v_x=-2\rho g\frac{\partial h}{\partial x}\int_z^H \hat{E}(\mathcal{A})A(T')\,\sigma^{n-1}\,\bar{z}\ \mathrm{d}\bar{z}, \tag{12}$$

where H is the ice thickness. The slip vanishes at the ice base, thus $v_x(H)=0$. Moreover, v_y vanishes per definition of the coordinate system and the vertical velocity v_z results from integrating the prescribed vertical strain rate D_{zz}. The latter is constant from the free surface down to two thirds of the ice thickness. Below, D_{zz} is linearly decreasing in such a way that the the downward vertical velocity v_z equals the accumulation rate at the surface. A similar distribution is employed for the temperature T': at the top, we set $T'=228.55$ K for $z=0,\dots,2/3\times$ depth. Further downwards, the temperature T' decreases linearly such that $T'(\text{bottom})=273.15$ K.

Horizontal extension is parameterized by

$$\begin{aligned} D_{xx} &= \frac{\partial v_x}{\partial x}=-aD_{zz}, \\ D_{yy} &= \frac{\partial v_y}{\partial y}=-[1-a]D_{zz}. \end{aligned} \tag{13}$$

In case of isotropic extension, the parameter $a\in[-1,1]$ is equal to $1/2$ and equal to unity for extension in the x-direction only (pure shear). The horizontal shear rate $\gamma:=\partial v_x/\partial z$ results from Eq. (12) and depends on the deformability $\mathcal{A}$,

$$\gamma=2\rho g\frac{\partial h}{\partial x}\,\hat{E}(\mathcal{A})\,A(T')\,\sigma^{n-1}\,z. \tag{14}$$

As mentioned above, the surface is isotropic because the ice crystallites are randomly distributed at the top. Therefore, we set $\mathcal{A}_{\text{surface}}=1$.

4 Numerical procedure

Our main interest is to simulate the ice flow, especially the development of the anisotropic fabrics. Therefore, the distribution of the orientations is of particular interest. As a governing equation, we discretize the orientation mass balance, i.e. Eq. (1). Since the total time period for Antarctic ice is very large, it is reasonable to assume that the orientation mass density ρ^* is time-independent. Moreover, the drilling site has a diameter of 10 cm. Consequently, ρ^* depends neither on the x nor on the y coordinate. This leaves us with $\rho^*=\rho^*(z,\boldsymbol{n})$:

$$\frac{\partial\rho^*}{\partial z}v_z+\mathrm{div}_{S^2}(\rho^*\boldsymbol{u}^*)=\rho^*\Gamma^*. \tag{15}$$

In [11] only two out of the four recrystallization effects, namely local rigid body rotation and grain rotation are implemented in the numerical scheme. In this contribution, we account for all four effects. However, the data gained at the EDML drilling site shows that the formation of subgrain boundaries and, thus, polygonization play an important role in ice-sheet deformation and may not be neglected [13].

Eq. (15) is discretized with a finite volume method, where we introduce spherical coordinates. The polar angle θ and the azimuth angle φ both have a uniform resolution of $\Delta\theta=\Delta\varphi=5^\circ$. In the z direction, the resolution is refined with depth via $z_{i+1}=z_i+(v_z)_i\Delta t$, where $z(0)=0$ at the surface, $(v_z)_i$ is the vertical velocity at depth z_i and we choose $\Delta t=1$ day.

5 Computational modeling

5.1 Material parameters

An experimental determination of the diffusivity λ and the material parameter Γ_c is rather difficult. The relevant time scales are too large and the strain rates are too low in order to be easily reproduced in the laboratory. However, it is known that at the EDML site the vertical strain rate D_{zz} is of magnitude order 10^{-5} per year (see e.g. [14]). Thus, the diffusivity should be approximately of order $10^{-14}\ \mathrm{s}^{-1}$. In particular, we choose one order less: $\lambda = 1.0 \cdot 10^{-15}\,\mathrm{s}^{-1}$ for the orientation diffusivity. Moreover, the constitutive parameter Γ_c should be of approximately the same order. We therefore set $\Gamma_c = 1.0 \cdot 10^{-15}\,\mathrm{s}^{-1}$. [11] achieve a best fit for a shape factor $\iota = 0.6$ which we henceforth adopt. Thus, the local rigid body rotation contribution predominates over the the grain rotation.

The stress exponent $n = 3$ is given in e.g. [6, 12] for the isotropic version of Glen's flow law. As mentioned above, the maximum enhancement factor $E_{\max} = 10$ and the minimum enhancement factor $E_{\min} = 0$, see the experiments of e.g. [10]. As usual, the universal gas constant reads $R = 8.314\,\mathrm{J\,mol^{-1}K^{-1}}$ and the gravity acceleration is $g = 9.81\,\mathrm{m\,s^{-1}}$. Last but not least, the melting temperature at zero pressure is of course $T_0 = 273.16\,\mathrm{K}$.

From experimental data (e.g. [3, 14]) we conclude that the horizontal strain field shows extension lateral to the flow direction and smaller compression in longitudinal direction. Thus, we choose $a = -0.3$ such that $D_{xx} = 0.3\,D_{zz}$ and $D_{yy} = -1.3\,D_{zz}$ and the incompressibility condition $D_{xx} + D_{yy} + D_{zz} = 0$ is fulfilled.

5.2 Numerical results: uniaxial vertical compression

In this paper, we discuss the case of uniaxial vertical compression. Consequently, the horizontal shear rate $\gamma = 0$ vanishes.

Down to 500 m a uniform orientation distribution is observed, see Fig. 3. This corresponds to an isotropic fabric as usually found in the upper regions. A significant preferred crystal elongation direction cannot be seen. Below 600 m, the ice crystallites start to orientate themselves in a preferred direction and a so-called girdle developes, see Fig. 3. Further down, from 2250 m downwards, a single maximum fabric along the vertical core axis develops. A strong single-maximum fabric forms in the near-basal parts of the core.

Fig. 1 shows the variation of the enhancement factor $\hat{E}(\mathcal{A})$ (see Eq. (9)) along the ice core. In the beginning it is close to unity which reflects that the fabric is approximately isotropic in that region. Further down, the fabric develops towards a girdle resulting in an enhancement factor close to 0. Consequently, in those depths, the fabric produces a significantly different mechanical response depending on the girdle's orientation. Further down, a single maximum develops with its crystal basal planes orientated in such a way that large deformations arise. Consequently, the enhancement factor increases sharply. The crystal basal planes are favorably orientated for the now prevailing simple-shear deformation. Moreover, the ice fluidity increases in this region.

The evolution of the symmetric orientation tensor $\boldsymbol{a}^2$

$$\boldsymbol{a}^2(\boldsymbol{x},t) := \int_{S^2} f^*(\boldsymbol{x},t,\boldsymbol{n})\boldsymbol{n}\otimes\boldsymbol{n}\,\mathrm{d}^2n, \qquad (16)$$

which is calculated in a post-processing step, is illustrated in Fig. 2. A large value of a_{33} represents a concentration of the grains in vertical direction. An ideal single maximum fabric would result in $a_{33} \to 1$. a_{11} and a_{22} indicate the symmetry with respect to the vertical direction in the sense that if $a_{11} = a_{22}$ the cross section is symmetric and $|a_{11} - a_{22}|$ represents the degree of anisotropy. The development of a_{33} illustrates the fabric's evolution from isotropy to an anisotropic single maximum close to the core bottom.

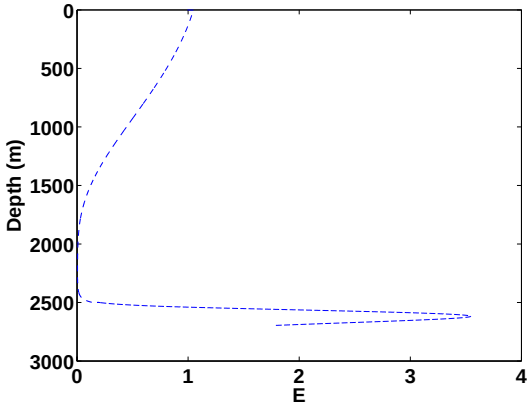

Figure 1: Variation of the enhancement factor $\hat{E}(\mathcal{A})$ along the EDML ice core. An enhancement factor $\hat{E}(\mathcal{A})$ close to unity represents an isotropic fabric in that region. Between 1750 m and 2450 m the enhancement factor $\hat{E}(\mathcal{A})$ is close (but not equal) to zero indicating the formation of a girdle.

6 Conclusion

Primarily, the deep drilling site in Antarctica was established in order to gain climate information. Different deformation modes affect the different time sequences. Therefore, the flow history of the ice is of

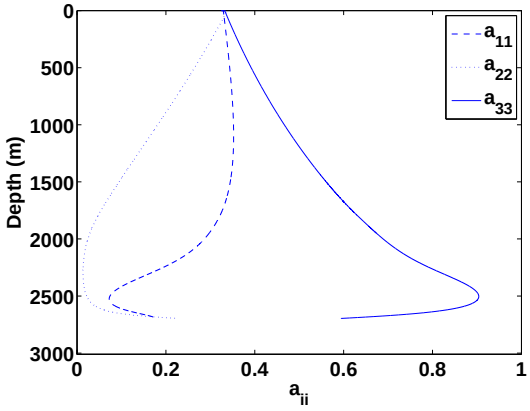

Figure 2: Variation along the EDML ice core of the three diagonal components of the second-order orientation tensor $\boldsymbol{a}^2$.

major significance. In this contribution, the relatively newly introduced CAFFE model is applied. The primary goal is the modeling of the ice flow in order to understand the deformation process the ice sheet has been exposed to. The underlying microstructure influences this process and has to be taken into account. The CAFFE model is a continuum mechanical approach which considers the microstructure indirectly.

First numerical results for the CAFFE model are presented in Seddik et al. [11]. However, only two out of the four recrystallization effects (local rigid body rotation and grain rotation) are considered. The results of Seddik et al. [11] show that the CAFFE approach captures the basic tendency of the ice to first develop a girdle and, subsequently, a single maximum. However, without the two remaining recrystallization effects there exist (i) numerical problems below 2100 m and (ii) the numerical simulations and the experimental data deviate in some points. Thus, it is critical to neglect grain boundary rotation and grain recrystallization, especially in the depth. In this contribution, we account for all four effects. In particular, migration recrystallization drives the fabric back towards a vertical single maximum which is most favorable for bed-parallel simple-shear deformations.

The CAFFE model is capable of modeling anisotropic ice flow in thick ice masses. Due to its simple structure and the fact that it takes the microstructure into account indirectly, computational time is rather small.

Acknowledgements: S.B. was supported by grant BA 3951/1 of the German Science Foundation (DFG) which is gratefully acknowledged. This research was done while S.B. visited Hokkaido University whose hospitality is also gratefully acknowledged.

References:

[1] N. Azuma, A. Higashi, Formation processes of ice fabric pattern in ice sheets, *Ann. Glaciol.*, 6, 1985, 130–134.

[2] N. Azuma, A flow law for anisotropic polycrystalline ice under uniaxial compressive deformation. *Cold Reg. Sci. Technol.*, 23(2), 1995, 137–147.

[3] O. Eisen, S. Kipfstuhl, D. Steinhage, F. Wilhelms, Direct evidence for continuous radar reflector originating from changes in crystal-orientation fabric, *Cryosphere*, 1, 2007, 1–10.

[4] A.J. Gow, T. Williamson, Rheological implications of the internal structure and crystal fabrics of the West Antarctic ice sheet as revealed by deep core drilling at Byrd Station. *CRREL Rep.*, 76(35), 1976, 1665–1677.

[5] F. J. Humphreys, M. Hatherly, Recrystallization and Related Annealing Phenomena. Elsevier, 2004.

[6] W.S.B. Paterson, The Physics of Glaciers. Pergamon Press, Oxford etc., 3rd ed. 1994.

[7] L. Placidi, K. Hutter, Thermodynamics of polycrystalline materials treated by the theory of mixtures with continuous diversity. *Cont. Mech. Thermodyn.*, 17(6), 2006, 409–451.

[8] L. Placidi, R. Greve, H. Seddik, S.H. Faria, A continuum-mechanical, anisotropic flow model for polar ice, based on an anisotropic flow enhancement factor. *Cont. Mech. Thermodyn.* 2009; doi: 10.1007/s00161-009-0126-0

[9] J.-P. Poirier, Creep of crystals, Cambridge University Press, 1985

[10] D.S. Russell-Head, W.F. Budd, Ice sheet ow properties derived from borehole shear measurements combined with ice core studies. *J. Glac.*, 24(90), 1979, 117–130.

[11] H. Seddik, R. Greve, L. Placidi, I. Hamann, O. Gagliardini, Application of a continuum-mechanical model for the flow of anisotropic polar ice to the EDML core, Antarctica. *J. Glac.*, 45(187), 2008, 631–642.

[12] C.J. van der Veen, Fundamentals of Glacier Dynamics. A. A. Balkema, Rotterdam, The Netherlands. 1999

[13] I. Weikusat, S. Kipfstuhl, S.H. Faria, N. Azuma, A. Miyamoto, Subgrain boundaries and related microstructural features in EDML (Antarctica) deep ice core, *J. Glac.*, 55, 2009, 461–472

[14] C. Wesche, O. Eisen, H. Oerter, D. Schulte, D. Steinhage, Surface topography and ice flow in the vicinity of the EDML deep-drilling site, Antarctica, *J. Glac.*, 53(182), 2007, 442–448.

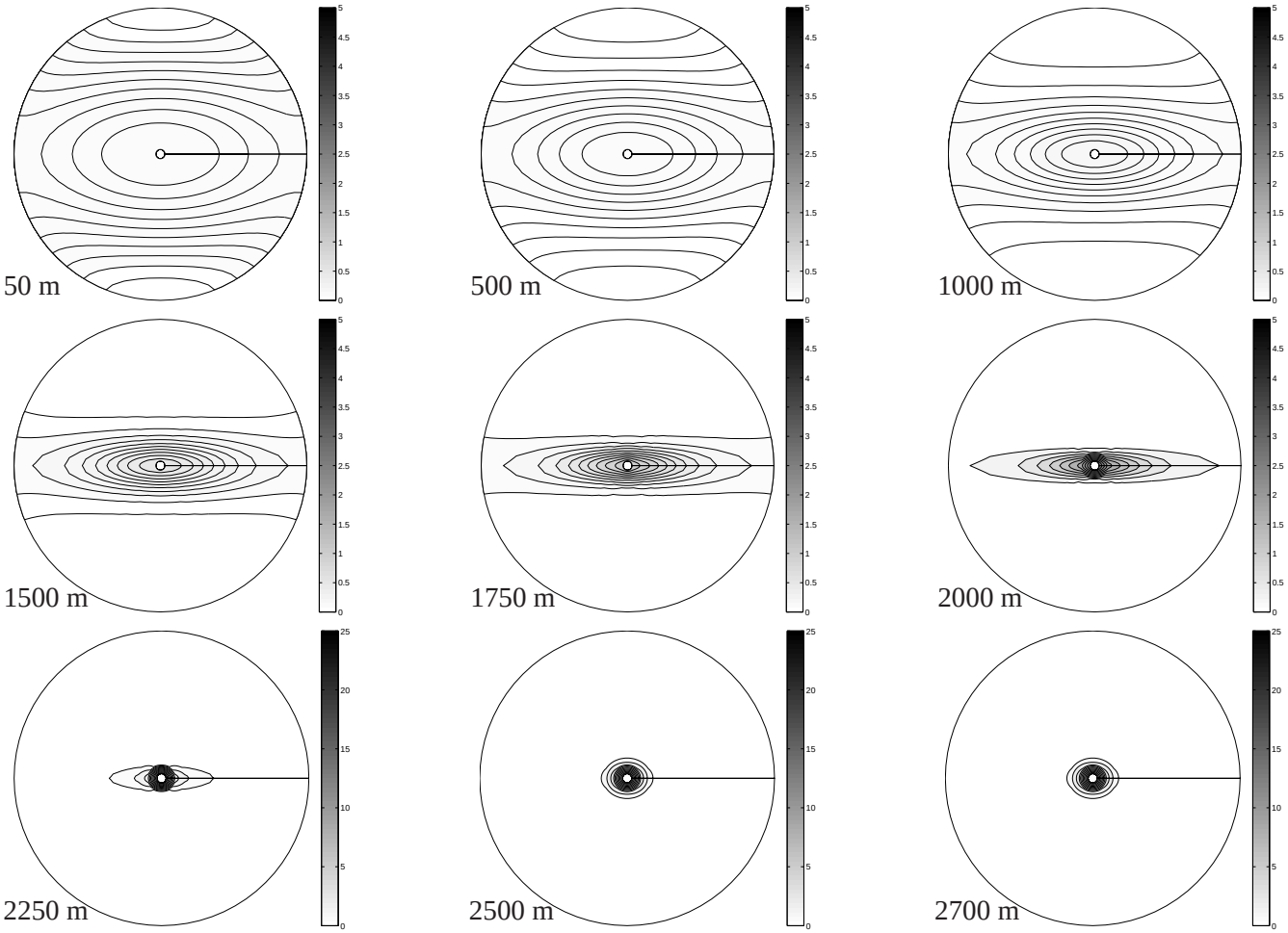

Figure 3: Schmidt diagram representation of the EDML fabrics (ρ^*/ρ) at depths between 50 m and 2700 m. The centres of the diagrams coincide with the core axis. The intersection of an orientation $\boldsymbol{n}$ with its unit sphere S^2 is projected onto the centered circular cross section (the horizontal x-y-plane). Consequently, a vertical orientation is plotted in the center and an orientation lying flat is plotted on the edge. In the beginning (50 m - 500 m) an isotropic fabric is seen. At approximately 1000 m, a girdle develops. From 2250 m onwards, a single maximum (representing a complete anisotropic fabric) exists.